Albedo Feedback, the Meridional Structure of the Effective Heat Diffusivity, and Climatic Sensitivity: Results from Dynamic and Diffusive Models

ISAAC M. HELD AND DAVID I. LINDER

Geophysical Fluid Dynamics Laboratory/NOAA, Princeton University, Princeton, NJ 08540

MAX J. SUAREZ

Department of Atmospheric Sciences, University of California, Los Angeles 90024

(Manuscript received 9 February 1981, in final form 20 April 1981)

ABSTRACT

The sensitivity of a two-level primitive equation atmospheric model to solar constant perturbations is examined in the presence of surface albedo feedback. The model is simplified to the point that a large number of numerical experiments can be performed and statistically steady states defined with relative ease. Exceptionally sensitive equilibrium states are found that are unrelated to the large and small ice-cap instabilities obtained in the simplest diffusive energy balance models. Similar results are produced in a two-level diffusive model closely patterned after the dynamic model, and in a more highly idealized one-level model, by choosing a diffusivity with pronounced meridional structure resembling that of the effective diffusivity of the dynamic model. Sensitive states occur in the diffusive models when the albedo gradient enters the region equatorward of 60° in which the effective heat diffusivity of the atmosphere increases with increasing latitude.

1. Introduction

Energy balance considerations suggest that climatic sensitivity to perturbations in the solar constant (or to other radiative perturbations) is significantly enhanced by the positive feedback between temperature changes and albedo changes due to modification of ice and snow cover. Energy balance models predict further that the strength of this positive feedback increases as the solar constant decreases, to the point that the feedback becomes sufficiently strong to overcome all restoring forces and produces unstable growth of the ice and snow. Much of the interest in energy balance models results from the startling proximity in these models of the present climate to this "large ice-cap instability." Estimates of the decrease in the solar constant required for instability vary considerably from model to model, however, ranging from less than 2% in the original calculations of Budyko (1969) and Sellers (1969) to 10% or more in several recent calculations (Oerlemans and van den Dool, 1978; Hartmann and Short, 1979; Wang and Stone, 1980).

The growing importance of albedo feedback for climatic sensitivity as the climate cools is also clearly seen in the results obtained by Wetherald and Manabe (1975) using an atmospheric general circulation model. Because of the computational requirements of their model, these authors did not examine the character of the large ice-cap instability in any detail, but their Fig. 5 indicates that albedo feedback is rapidly increasing in strength when the solar constant is lowered to 1.92 ly min^{-1} (1340 W m^{-2}). Wetherald (personal communication) found that at 1.88 ly min^{-1} (1310 W m^{-2}) the ice cap slowly continued to expand for as long as it was practical to continue the numerical integration. These calculations seem to confirm the qualitative behavior found in the simpler models: over the range of solar constants considered, at least, sensitivity increases monotonically as the solar constant is lowered.

We describe here the response of a two-level primitive equation model on a sphere to solar constant variations. The computational requirements of the model are sufficiently small that climatic statistics are relatively easy to define and a large number of statistically steady states can be obtained. We utilize this model to study the large ice-cap instability and other effects of albedo variations on climatic responses. A detailed description of the model, along with our rationale for the various approximations made and a discussion of the model's limitations, can be found in Held and Suarez (1978, hereafter referred to as I). The sensitivity of this model to solar constant variations when the surface albedos are fixed has been analyzed in Held (1978, referred to as II). We now simply set the surface albedos equal to a particular function of surface temperature

0022-4928/81/091911-17$08.25

designed to approximate the effects of ice and snow cover, and reexamine the model's responses. The quantitative results described below depend on our crude radiative parameterization and are undoubtedly distorted somewhat by the two-level approximation and severe spectral truncation, as well as by the more obvious approximations of fixed cloudiness, no seasonal variation and no oceanic heat transport. We believe that these results are of interest, however, because the qualitative behavior of the model as the solar constant is varied is unlike that found in the diffusive energy balance models described in the literature. When the solar constant is decreased a few percent, pushing the albedo gradient at the ice-cap boundary equatorward of 60°, the model climate becomes extremely sensitive to the value of the solar constant, but this sensitivity is not a sign that the large ice-cap instability is close at hand. Instead, as the solar constant is lowered further, the model climate becomes less rather than more sensitive. These relatively stable large ice-cap states exist for a range of ~5% of the solar constant. For still lower values of the solar constant the large ice cap becomes unstable and covers the planet.

The simple "Hadley adjustment" model of Lindzen and Farrell (1977) is capable of producing similar non-monotonic changes in sensitivity as the solar constant is lowered. However, the non-monotonic changes in sensitivity in our model do not seem to be related to the Hadley cell. Rather, they are closely related to the meridional structure of the poleward heat flux in middle and high latitudes. This becomes clear when we mimic the primitive equation calculations with an energy balance model. As described in Section 4, this simple model produces very sensitive climates when the ice-cap boundary penetrates into the region (60–40° latitude) in which the effective meridional heat diffusivity of the atmosphere increases rapidly with increasing latitude. After the ice cap passes through this region, the sensitivity of the model decreases. When the latitudinal structure of the diffusivity is removed from the energy balance model, the sensitive region disappears and one is left with a simple monotonic increase in sensitivity with decreasing solar constant, except for a very weak remnant of the small ice-cap instability which is sensitive to the structure of the diffusivity near the pole.

2. The primitive equation model

The dynamic model utilized is a two-level primitive equation model on a sphere, in which all fields are Fourier analyzed in the zonal direction and very severely truncated, retaining only wavenumbers 0, 3 and 6. Potential temperature is a prognostic variable at both levels, so that the static stability of the atmosphere is predicted. Water vapor mixing ratio is carried as a prognostic variable at the lower level only. The lower boundary is assumed to be a swamp —a flat, water-saturated, zero heat capacity surface. Insolation at the top of the atmosphere is fixed at its annual mean value as a function of latitude. The equations are solved by finite-differencing in the meridional direction using a staggered 3° latitude grid, placing the boundaries at ±84° latitude, and integrating forward in time with a semi-implicit step.

The model's zonally averaged temperature equations can be written in the form

$$\left.\begin{aligned}\frac{\partial \Theta_1}{\partial t} &= R_1 + \left(\frac{p_*}{p_1}\right)^{\kappa} \times [Q_1^{\mathrm{LW}} + Q_1^{\mathrm{SW}} + Q^{\mathrm{CONV}}] + \epsilon_1 \\ \frac{\partial \Theta_2}{\partial t} &= R_2 + \left(\frac{p_*}{p_2}\right)^{\kappa} \times [Q_2^{\mathrm{LW}} + Q_2^{\mathrm{SW}} + Q^{\mathrm{SH}} + Q^{\mathrm{LH}} - Q^{\mathrm{CONV}}] + \epsilon_2\end{aligned}\right\}. \quad (1)$$

Subscripts 1 and 2 refer to the upper and lower levels, respectively. Θ_i is the proportional temperature and R_i the convergence of the large-scale (horizontal and vertical) fluxes of potential temperature, while $p_* = 1000$ mb, $p_1 = 250$ mb, $p_2 = 750$ mb, and $\kappa = 2/7$. Q_i^{LW} and Q_i^{SW} are the long-wave and short-wave heating rates. In order to complete the description of the radiative calculation provided in I, and in order to correct several errors in Table 2 in I, the computation of Q_i^{LW} and Q_i^{SW} is described in full in Appendix A. The computation of the sensible heating Q^{SH}, the latent heat release in the lower layer Q^{LH}, and the heat transported upward by the convective adjustment Q^{CONV} are completely described in I. The term ϵ_i represents the sum of two very small effects—a nonlinear subgrid-scale diffusion, also described in I, and the small amount of heat released when kinetic energy is dissipated.

The model is identical to the two-wave, $m = 3$–6, moist version of the model utilized in I and II, except for the following two changes:

1) Most importantly, the surface albedo γ is now chosen to be the following function of surface temperature T_*:

$$\gamma = \begin{cases} 0.1, & 273 < T_* \\ 0.1 + 0.6 \times (273 - T_*)/20., & 253 < T_* < 273 \\ 0.7, & T_* < 253. \end{cases} \quad (2)$$

As discussed in I, in Section 2d, the model's surface temperature is a function of time and latitude only. Surface albedo variations are therefore independent of longitude. Using the crude model described in Appendix A, a surface albedo of 0.1 (0.7) typically results in a planetary albedo of 0.34 (0.68). Changes

in surface albedo have roughly the same effect on planetary albedo at all latitudes in this model, very likely one of its more serious deficiencies.

Our primary reason for choosing this smooth transition from ice-free (0.1) to ice-covered (0.7) surface albedos is that we want to avoid the small ice cap instability present in discontinuous albedo models (Held and Suarez, 1974; North, 1975). Numerical solutions to the simplest diffusive models with smoothed rather than discontinuous albedos show that even a modest smoothing of the ice-free to ice-covered transition is sufficient to destroy the small ice cap instability, whereas smoothing as substantial as that in (2) has little effect on the large ice-cap instability. A remnant of the small ice-cap instability can still be discerned in the continuous albedo models, however, and a brief discussion of this point is included in Appendix B. It is clear, in any case, that a useful analysis of the stability of the Arctic or Antarctic ice caps to melting would take explicit account of the seasonally varying solar flux. The choice of a smooth albedo-temperature relation allows us to concentrate on the character of the large ice-cap instability and the effects of small, relatively stable ice caps on climatic responses.

2) In the calculations described in I and II, the heat released on dissipation of kinetic energy is ignored. Globally averaged, this source of heat amounts in the model to less than 3 W m^{-2}. A 10% change in solar constant, or roughly a 25 W m^{-2} change in mean solar heating, results in less than 1.0 W m^{-2} change in dissipative heating when albedos are fixed, so the effect of this simplification on the climatic responses described in II is extremely small. If, however, the model undergoes an abrupt transition in which frictional dissipation increases by a substantial fraction of itself when the solar constant is changed by a small amount, then significant distortion of the response can occur. Since a transition of this sort does occur in the present calculations, we now include this heating due to frictional dissipation in the model. Experiments without this heating term show, as expected, that its omission does have some effect, but that the qualitative character of the responses is unchanged.

3. Results

Numerical experiments at 18 values of the solar constant are summarized in Table 1. The integrations are of varying lengths, and climatic statistics are gathered from the final 400, 800 or 1200 days of each integration. Initial conditions are the final states from other runs, as listed in the table. Several experiments of somewhat shorter duration were performed using different initial conditions to check for non-uniqueness of the equilibrium states, but none was found. (The model's ice-covered earth solution, which is undoubtedly stable over this range of solar constants, has not been examined.) Zero percent refers to a solar constant of 1395 W m^{-2}, this being the case which produces a surface temperature distribution closest to the observed (see Fig. 4a). Our radiative model evidently has a small cold

TABLE 1. Experiments performed with the dynamic model. $Q = x\%$ should be read $Q = [1 + (0.01)x]Q_0$, with $Q_0 = 1395$ W m^{-2}. The "initial condition" column indicates that calculation the final state of which is utilized as the initial state of the calculation with solar constant Q. $0\%f$ refers to the fixed albedo calculation described in II. The final three columns are the global mean surface temperature, planetary albedo and eddy kinetic energy. The $Q = -6\%$ case is still cooling rapidly at day 1600.

Q	Length of integration (days)	Averaging period (days)	Initial condition	T_s (K)	Planetary albedo	EKE (m s^{-1})^2
+8%	800	400	+6%	296.86	0.3288	37.5
+7%	800	400	+6%	296.10	0.3295	37.6
+6%	800	400	+4%	295.37	0.3303	38.2
+5%	800	400	+4%	294.49	0.3310	37.4
+4%	800	400	0%f	293.54	0.3321	37.0
+3%	800	400	0%f	292.62	0.3339	38.4
+2%	1200	400	0%f	291.39	0.3363	37.8
+1%	1200	400	0%f	290.02	0.3399	38.4
0%	1200	400	+1%	287.47	0.3589	42.0
−0.5%	1600	~	0%	~	~	~
−1%	2400	1200	0%	278.86	0.3904	50.8
−1.5%	2400	~	−0.5%	~	~	~
−2%	2400	1200	0%	272.01	0.4234	55.6
−3%	1600	800	−2%	266.33	0.4500	60.8
−4%	1600	800	−2%	260.95	0.4758	66.6
−5%	2000	800	−4%	254.94	0.5047	69.6
−5.5%	2400	800	−5%	251.37	0.5229	71.6
−6%	1600	~	−5.5%	233.00 at day 1600	~	~

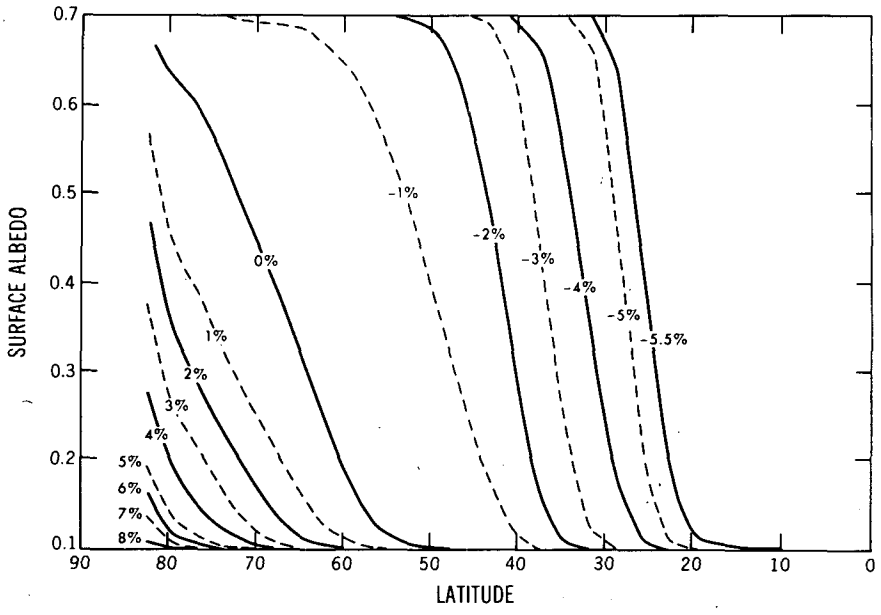

FIG. 1. Surface albedo as a function of latitude for different values of the solar constant.

bias. Time-averaged surface albedos are plotted in Fig. 1. The latitude of the ice-cap boundary is relatively insensitive to the value of the solar constant Q for $Q > +1\%$, extremely sensitive in the range $+1\% > Q > -2\%$, and then somewhat less sensitive once again for $-2\% > Q > -5.5\%$. At $Q = -6\%$ the ice cap advances unstably until it covers the planet.

Fig. 2 depicts the time evolution of the global mean potential temperature for the calculations with $+4\% > Q > -3\%$, spanning the region of exceptional sensitivity. Smoothing by eye has eliminated a small amount of high-frequency variability. The slow and large variation in the -0.5 and -1% calculations and the slow relaxation and decidedly nonexponential character of this relaxation in the -1.5

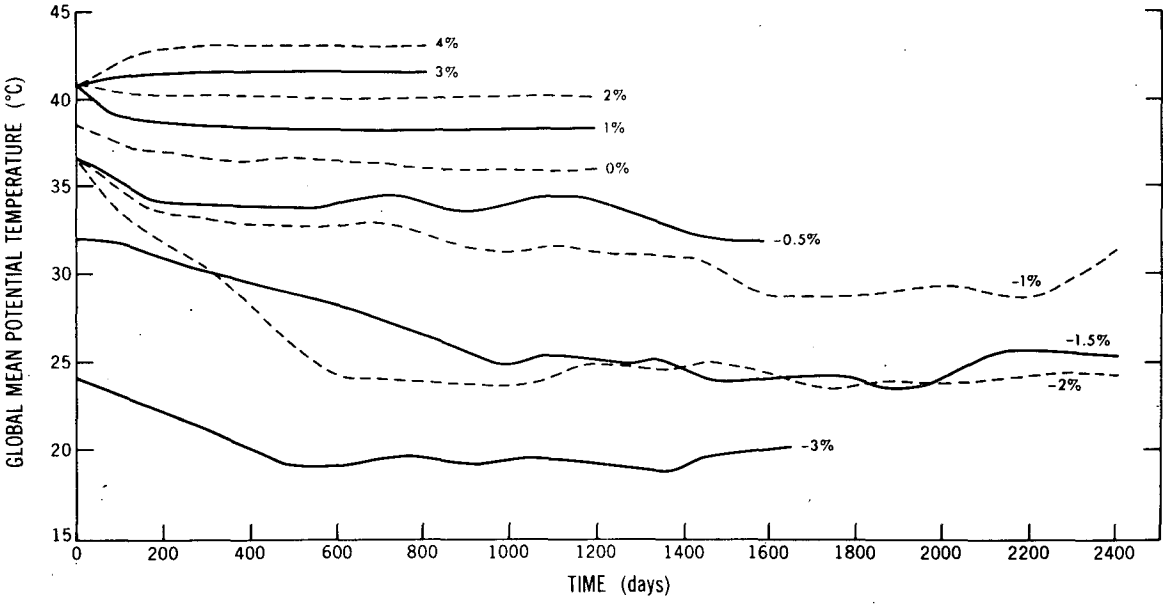

FIG. 2. Time evolution of the global mean potential temperature in several of the calculations, defined as the average over latitude of $\frac{1}{2}(\Theta_1 + \Theta_2)$. [The potential temperature at 500 mb obtained by linearly interpolating in $\ln(p)$ between the two model levels is typically 10 K warmer than $\frac{1}{2}(\Theta_1 + \Theta_2)$.]

and −2% calculations are particularly striking. For −2% one gets a strong impression that near day 600 the system passes from a region of slow relaxation and weak restoring forces into a region of relative stability. The lengths of the −0.5, −1 and −1.5% calculations clearly are insufficient for the adequate definition of statistically steady states. However, for the sake of continuity in the presentation of results, statistics for $Q = -1\%$ have been computed from the final 1200 days of the integration.

Changes in global mean surface temperature per percent change in solar constant, computed from neighboring values in Table 1, are plotted in Fig. 3. Also shown for comparison are the corresponding results obtained in the fixed albedo calculations described in II. The behavior of the sensitivity for $Q > -1\%$ is similar to that found in most energy balance models described in the literature, temperatures becoming more sensitive as the ice cap advances and albedo feedback strengthens. The sensitivity decreases as Q falls below −1%, however, and then rises again near the onset of the large ice-cap instability. The integrations are not of sufficient length to define the sensitivity near −1% very precisely. Because the −1.5 and −2% cases produce temperatures so similar in Fig. 2, we suspect, in particular, that the dip in sensitivity on the cold side of the sensitivity maximum may be more pronounced than indicated in Fig. 3.

Fig. 4a is a plot of the surface temperature as a function of latitude in the various calculations. Observed annual mean Northern Hemisphere atmospheric temperatures at 1000 mb (from Oort and Rasmussen, 1971) are also indicated. Temperature changes per percent change in solar constant, computed using the +8, +6, +4, +2, 0, −2 and −4% calculations, are plotted in Fig. 5a. The sensitivity of the fixed albedo model (computed using the +10 and 0% cases) is once again shown for comparison. Even when surface albedos are fixed, variations in static stability result in the model's surface temperatures being twice as sensitive in high as in low latitudes, as noted in II. Albedo variations amplify this tendency, as expected. In the 0 to −2% transition shown in the figure, the temperature response at 60° is six times larger than the response at the equator. These surface temperature results give the impression that the tropics are reasonably well insulated from the dramatic events in high and middle latitudes. However, similar plots of mean atmospheric temperatures in Figs. 4b and 5b demonstrate that this impression is misleading: the model's mean atmospheric temperatures in high and low latitudes are very strongly coupled. Changes in mean atmospheric temperature gradients are much smaller than changes in surface temperature gradients, implying pronounced changes in static stability.

The static stability variations are shown explicitly in Fig. 6, a plot of $\frac{1}{2}(\Theta_1 - \Theta_2)$. The decrease in static stability in low latitudes with decreasing insolation follows from the decrease in the stability of a moist adiabat with decreasing temperature. The point marking the boundary between latitudes at which the stability decreases and latitudes at which

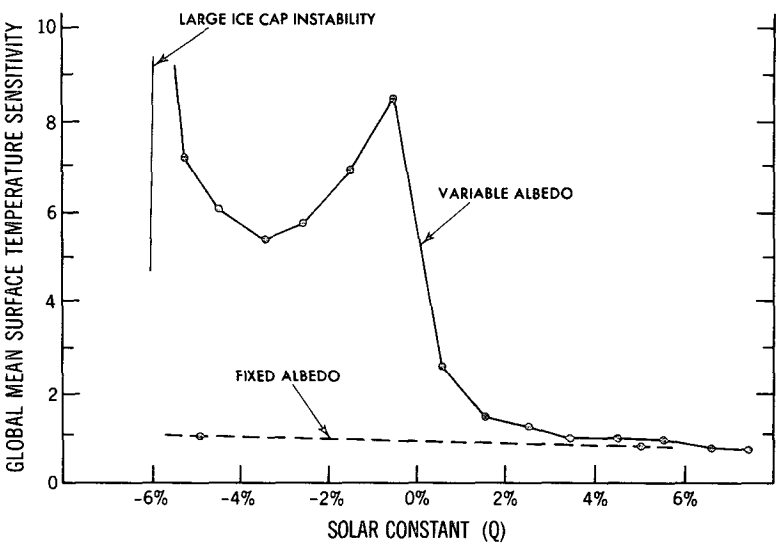

FIG. 3. The sensitivity of global mean surface temperature to perturbations in solar constant Q, plotted against Q. Fixed albedo results computed from the $Q = -10$, 0 and +10% experiments described in II are shown for comparison. The temperature sensitivity is normalized to correspond to a change in Q of $0.01Q_0$. (Q_0 = 1395 W m^{-2}.)

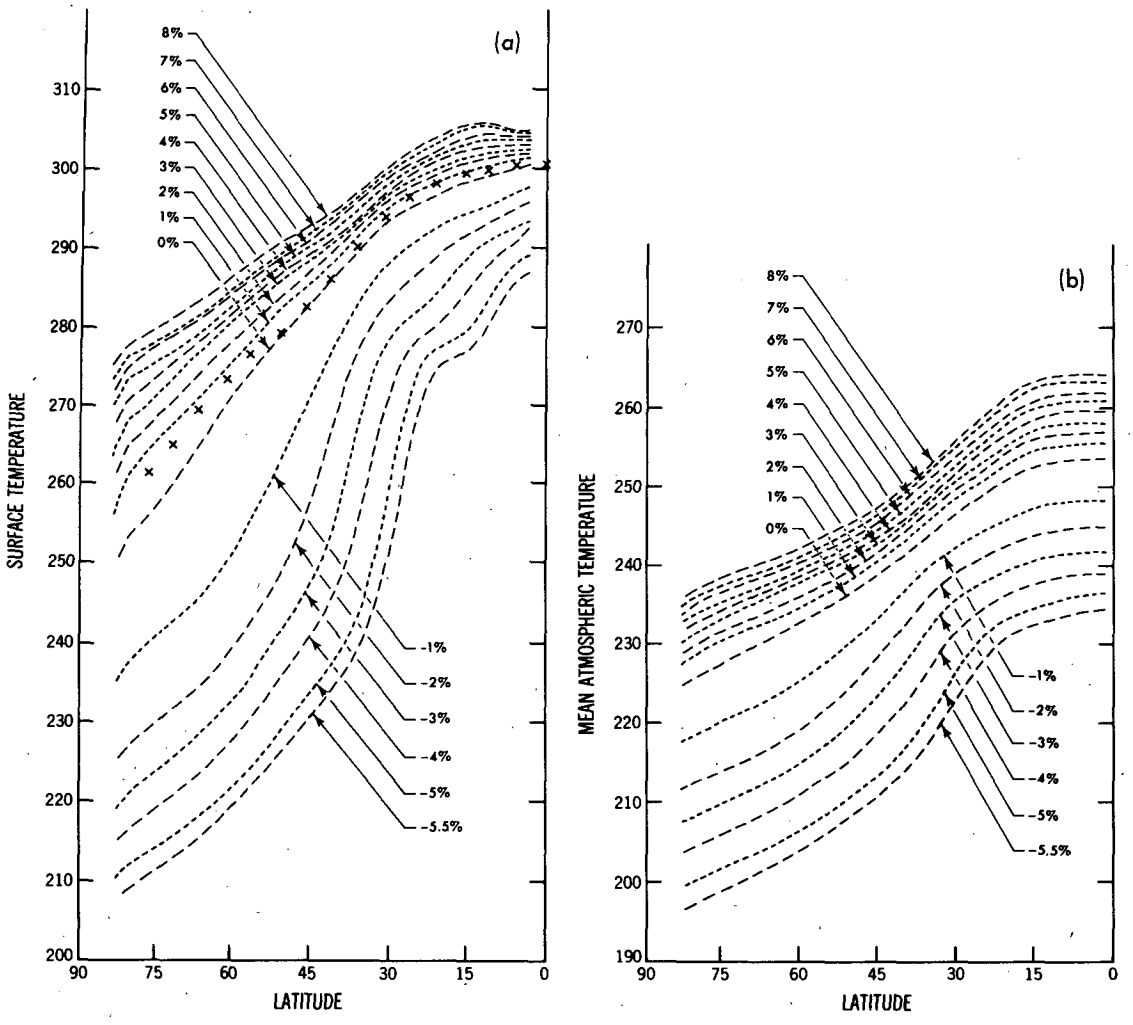

Fig. 4. (a) Surface temperature and (b) vertical mean atmospheric temperature, $0.5[(p_1/p_*)^\kappa\Theta_1 + (p_2/p_*)^\kappa\Theta_2]$, as functions of latitude for different values of Q. The observed surface temperatures are indicated by asterisks.

it increases moves equatorward as temperatures decrease, since the region within which moist convection is of importance shrinks toward the equator. The apparent insulation of the tropical surface from the events in higher latitudes is simply a result of these changes in stability.

The vertically averaged poleward energy flux (per unit length latitude circle) in a number of these calculations is displayed in Figs. 7a and 7b. The fluxes in the warmer cases (Fig. 7a) are sufficiently close to each other that the vertical scale has been amplified and only the region $30° < \theta < 65°$ is shown. As described in II, the total poleward flux decreases with decreasing solar constant when surface albedos are fixed, the bulk of the decrease being in the eddy latent heat flux. The same behavior is seen in the warmer cases in Fig. 7a. However, as the ice cap grows the meridional radiation gradient increases, driving larger eddies and larger sensible heat flux. In the range $-2\% < Q < +2\%$, the total energy flux increases with decreasing Q. Therefore, one can select two values of Q, on either side of $+2\%$, for which differences in sensible and latent heat fluxes of opposite sign nearly cancel, leaving the total flux unaffected ($+6$ and $+1\%$ are the best choice). This behavior is similar to that described by Wetherald and Manabe (1975) in their Fig. 14. If these authors had compared two warmer equilibrium states, one expects on the basis of Fig. 7 that the latent heat effect would have dominated and the total flux would have increased as the solar constant was raised. The flux responses in the CO_2 calculations by Manabe and Wetherald (1980, Fig. 5) confirm this expectation.

Fig. 7 indicates that a fairly small ice cap, extending only to 60° for $Q = +1\%$, can have a sub-

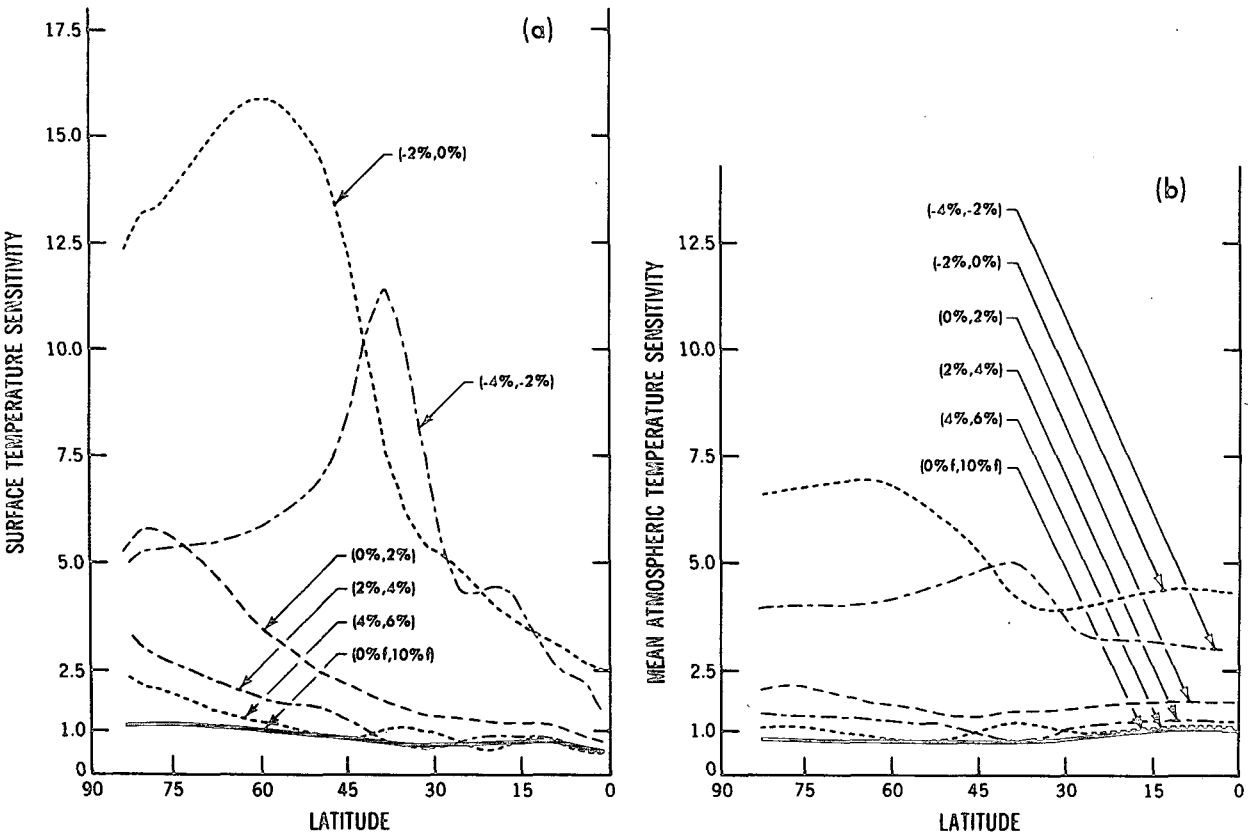

FIG. 5. (a) Surface temperature sensitivity and (b) vertical mean atmospheric temperature sensitivity as functions of latitude for different values of Q. The solid lines labelled ($0\%f$, + $10\%f$) are the sensitivities computed from the Q = 0% and +10% calculations in II, where f is the fixed albedo. Units are as in Fig. 3.

stantial effect on the total heat flux response throughout the hemisphere. Other dynamic responses of the model change qualitatively near $Q = +1\%$. One example is displayed in Table 1: the globally averaged eddy kinetic energy changes very little with decreasing Q for $Q > +2\%$, but increases sharply for $Q < +1\%$. {Based on the results in II, we expect $\partial(\mathbb{EKE})/\partial Q \approx 0.5$ [(m s^{-1})^2 per 1% change] when albedo feedback is negligible, but these small changes are apparently hidden by sampling errors in the warmer cases.}

The large changes in the model's total flux near the sensitivity maximum at $Q = -1\%$ are examined in more detail in Fig. 8. The total fluxes in the 0 and -2% calculations are split into three parts: the eddy sensible heat flux, the eddy latent heat flux, and the mean sensible plus latent heat flux. These fluxes are defined precisely as in II, p. 2094. As the system cools from 0 to -2%, the eddy sensible heat flux increases dramatically equatorward of 55° and decreases slightly poleward of 55°. The latter effect may in part be a consequence of the large increase in high-latitude static stability (Fig. 6) and the result-

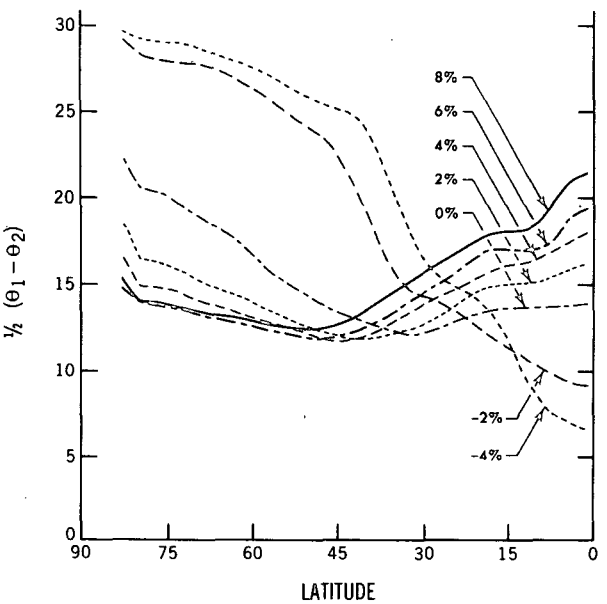

FIG. 6. Static stability ½($\Theta_1 + \Theta_2$) as a function of latitude for various values of Q.

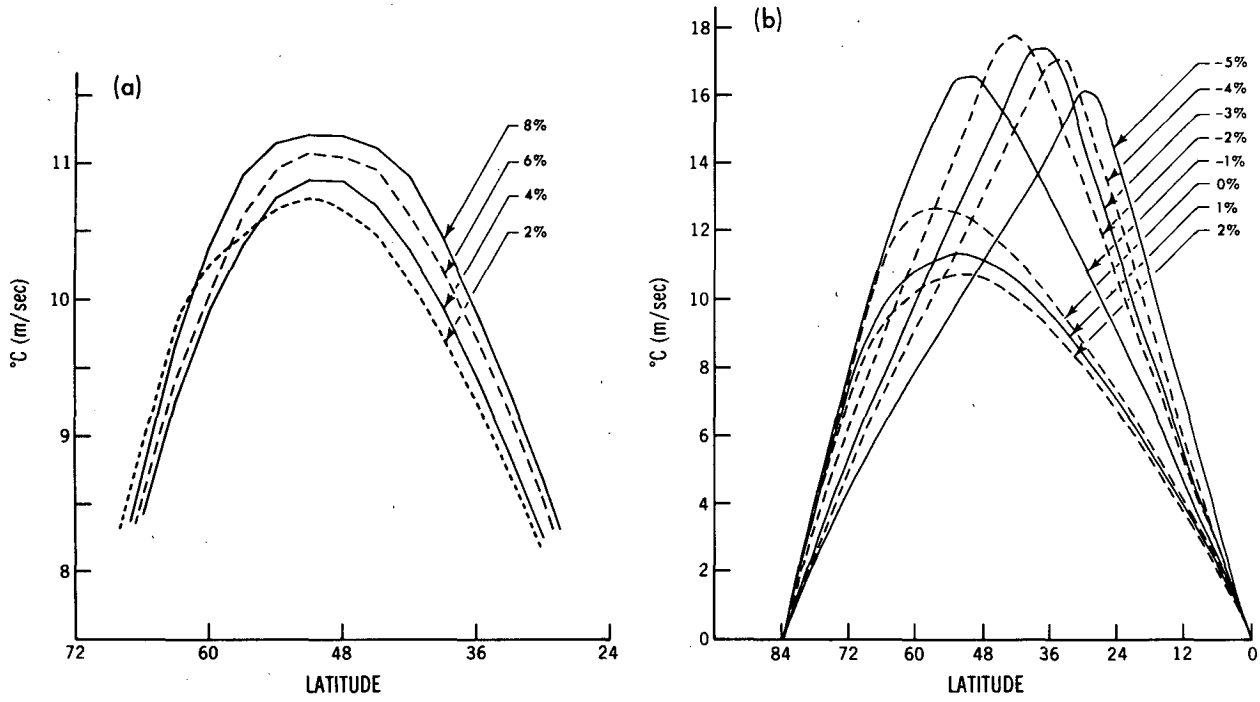

FIG. 7. Total poleward flux of energy per unit length of latitude circle. The full range of latitude is displayed for the colder cases (b). The warmer cases are plotted with magnified scales in (a). Values must be multiplied by $c_p = 10^3$ J (kg K)$^{-1}$ to obtain the energy flux.

ing weakening of the baroclinic instability of the flow. The eddy latent heat flux also decreases in high latitudes, but increases slightly equatorward of 45°. Evidently, the pronounced increase in eddy activity more than compensates for the decrease in temperature in the latter region (globally averaged eddy kinetic energy increases ≈30% in the transition from 0 to −2%). The most significant change in the heat flux due to the zonal mean flow is an increase in the equatorward flux in the Ferrel cell, centered near 40° in these calculations. There also is some increase in the flux in the polar direct cell, but the Hadley cell flux changes hardly at all. If one compares the vertically averaged atmospheric heating or cooling rates obtained from the convergences of these fluxes, one finds a large increase in cooling rate due to the eddy sensible flux in the −2% case (~0.4 K day^{-1}) at 35°, immediately in front of the advancing ice cap. However, roughly two-thirds of this increased cooling is compensated by the increase in the convergence of the Ferrel cell energy fluxes. The mean meridional circulation seems to be playing an important stabilizing role, counteracting the destabilizing effect of the increased eddy flux across the ice-cap boundary.

In any case, the largest changes in the heat transport by the mean circulation are well outside of the tropics, in regions in which one can obtain a good estimate of the model's zonal-mean meridional flow by dividing the convergence of the eddy momentum flux in the upper layer by the Coriolis parameter (since the upper layer's zonal acceleration by the Coriolis force is approximately balanced by this flux convergence—see Fig. 11 in I). If the atmosphere were dry, this balance would result in the sum of the eddy and mean meridional heat fluxes being proportional to the eddy potential vorticity flux in the upper layer (see II, p. 2088). In the analysis of this statistically steady flow, just as in a number of wave-mean flow interaction problems, the division of the total heat flux into eddy and zonal mean parts can be misleading.

4. Diffusive energy balance models

a. Two-level models

One can define an effective diffusivity for the dynamic model by dividing the total poleward energy flux per unit length of latitude circle F by the vertical mean atmospheric temperature gradient and by the heat capacity of an atmospheric column of unit cross section:

$$D \equiv -F\left(\frac{1000 \text{ mb}}{g}\,\frac{c_p}{a}\,\frac{\partial \bar{T}}{\partial \theta}\right)^{-1}. \qquad (3)$$

The values of $D(\theta)$ obtained for a number of calculations near the -1% sensitivity maximum are shown in Fig. 9. For $Q > -1\%$, the diffusivity increases from very small values near the polar boundary to a maximum near 60°, and then decreases to a minimum in the subtropics. The very small values of D near the pole are presumably in part a consequence of the absence of wavenumbers 1 and 2 from the model. The values of D in the tropics are not shown since they fluctuate wildly because of the small temperature gradients. After the system cools through the -1% transition, much of the latitudinal structure in D disappears. The time-averaged surface albedo in the -1% calculation is superimposed on Fig. 9 to show that the increase in sensitivity occurs when the sharp albedo gradient enters the region in which $\partial D/\partial\theta$ is large and positive.

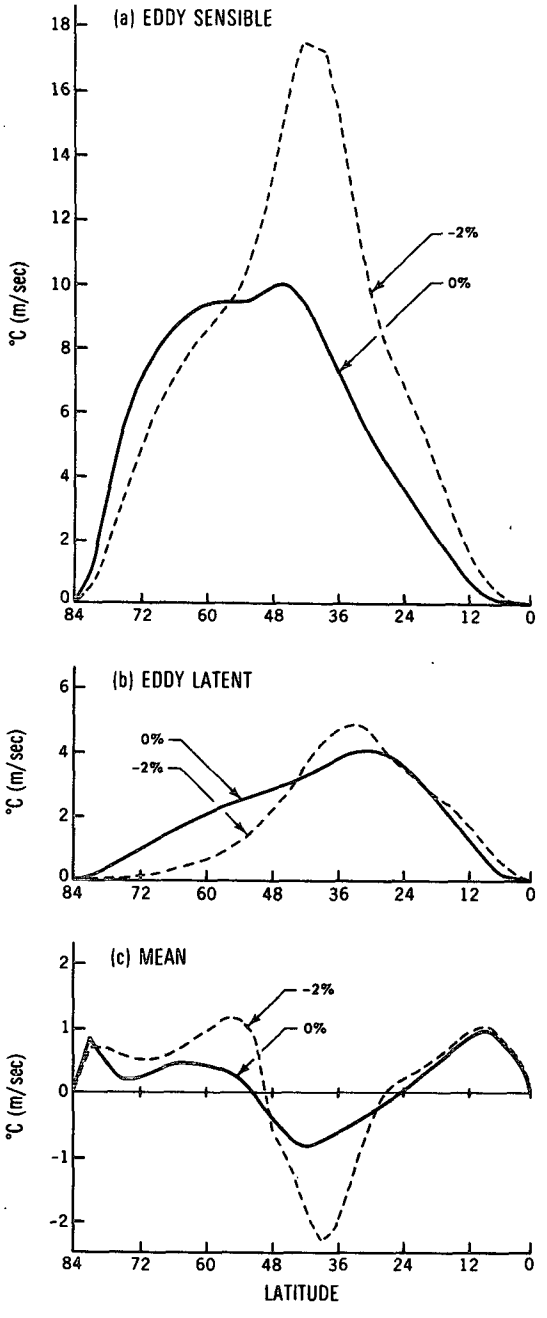

FIG. 8. The total poleward flux for $Q = 0$ and -2% divided into three parts: (a) eddy sensible heat flux; (b) eddy latent heat flux; and (c) sensible plus latent heat flux due to the mean meridional circulation.

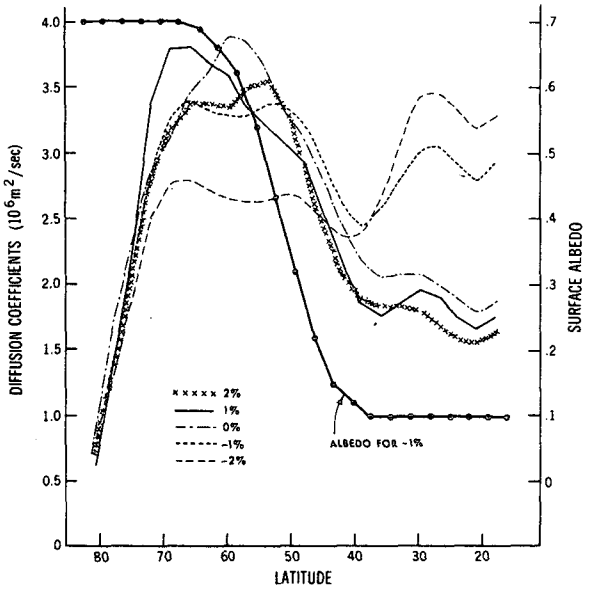

FIG. 9. The effective diffusivity as a function of latitude for five values of Q. Also plotted is the surface albedo distribution for $Q = -1\%$.

To confirm the impression one receives from Fig. 9 that this sensitivity maximum is related to the gradient of the effective diffusivity, we construct an energy balance model that closely resembles the dynamic model. The two potential temperature equations (1) are the only prognostic equations in the diffusive model. The dynamic heating, $R_i + \epsilon_i$, is simply replaced by

$$\frac{1}{a^2 \cos(\theta)} \frac{\partial}{\partial \theta} [\cos(\theta) D(\theta) \partial \Theta_i / \partial \theta], \qquad (4)$$

($a \equiv 6.4 \times 10^6$ m) using the same diffusion coefficient in both layers. This diffusive model therefore ignores the large-scale vertical flux of potential temperature present in the dynamic model. Calculations with a very similar diffusive model in Suarez and Held (1979) indicate that the moist convective adjustment and horizontal diffusion are jointly capable of maintaining reasonable static stabilities in a two-level model in the absence of the large-scale vertical flux, although the resulting model naturally under-

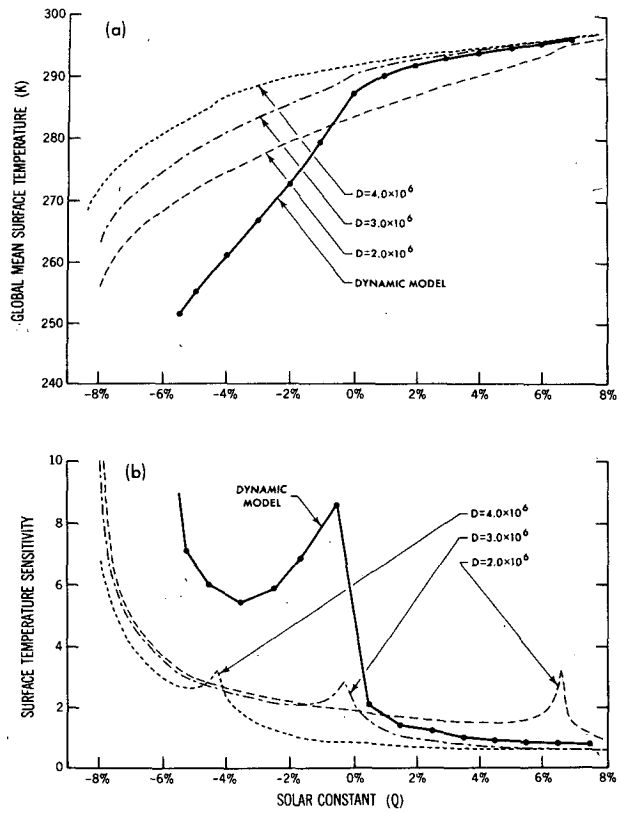

FIG. 10. Global mean surface temperatures (a) and surface temperature sensitivities to solar constant perturbations (b) as functions of Q, for the dynamic model and for several diffusive models with latitudinally uniform diffusivities. As in Fig. 3, temperature sensitivity is $\delta Q(\partial T/\partial Q)$ with $\delta Q = 0.01 Q_0$.

estimates the midlatitude stability somewhat. Since the vertical flux term changes in rather complex ways as the ice cap advances, and since we are already making substantial errors in the vertical distribution of the dynamic heating by using the same diffusion coefficient in both layers, we have chosen to omit the large-scale vertical flux in these diffusive calculations.

The sensible heat flux H and evaporation E from the surface are computed from

$$\left.\begin{aligned} H &= \alpha(T_A - T_*) \\ LE &= \frac{\alpha L}{c_p}[h_A r(T_A) - r(T_*)] \end{aligned}\right\}, \qquad (5)$$

where T_A is the atmospheric temperature at the ground (obtained by interpolating linearly in $\ln(p)$ from the two atmospheric temperatures); $h_A = 0.80$ is the relative humidity in the atmosphere at the ground; $r(T)$ is the saturation mixing ratio from Clausius-Clapyron, $c_p = 10^3$ J (kg °C)$^{-1}$, $L = 2.5 \times 10^6$ J kg^{-1} and $\alpha = 7$ W (m^2 °C)$^{-1}$. T_* is determined from the balance

$$S_\downarrow - H - LE = 0, \qquad (6)$$

where $S_\downarrow$ is the net downward radiative flux computed as in Appendix A. The sensible and latent heating of the lower layer are then determined from

$$(Q^{SH}, Q^{LH}) = (H, LE)/c, \qquad (7)$$

where

$$c \equiv c_p\,(500\text{ mb})/g = 5 \times 10^6\ [\text{J (m}^2\text{ K)}^{-1}].$$

Thus all evaporated water is condensed in the lower layer and at that latitude at which it evaporates. (By choosing D to fit the results for the total energy transport in the dynamic model, one is implicitly including latent heat transport in the diffusive term.) A convective adjustment does not allow $\Theta_1 - \Theta_2$ to drop below $\Theta_1^{ma} - \Theta_2^{ma}$, Θ_i^{ma} being the 250 and 750 mb potential temperatures on that moist adiabat with the same mean temperature, i.e.,

$$\tfrac{1}{2}[(p_1/p_*)^\kappa\Theta_1 + (p_2/p_*)^\kappa\Theta_2],$$

as the atmosphere being adjusted (see Fig. 3 in I). Surface albedos are again determined from (2).

All of these calculations are identical to those in the dynamic model except that in the latter model the coefficient α is dependent on lower layer wind speed, the relative humidity h_A is predicted by the model, and convective adjustment occurs only when the lower layer is saturated and is therefore sporadic. (In the steady state of the diffusive model, convective adjustment occurs continuously at a given latitude or it does not occur at all.) Also, in the dynamic model time-mean surface temperatures and albedos do not quite satisfy (2) because of variability in time; however, the difference only amounts to a slight rounding of the corners in the albedo-temperature curve. Similar slight differences resulting from time variability in the dynamic model occur in the radiative heating and boundary-layer calculations. All of these differences are minor, however, compared to the distortion of the vertical distribution of the dynamic heating in the diffusive model resulting from the absence of the large-scale vertical flux of potential temperature and from the choice of equal diffusivities in the two layers.

Figs. 10a and 11a compare the global-mean surface temperatures predicted by various versions of the diffusive model with those predicted by the dynamic model; Figs. 10b and 11b compare the changes in global mean surface temperature per percent change in solar constant. The results from diffusive models with latitude-independent diffusivities—2.0, 3.0 and 4.0 $\times 10^6$ m^2 s^{-1}—are plotted in Fig. 10. All of these constant-diffusivity models possess a large ice-cap instability near $Q = -8\%$. One evidently can associate the dynamic model's instability near -6% with this large ice-cap instability in the diffusive models. Thus, one should not think of the sensitive region near -1% as an incipient large ice-cap instability thwarted by the mean meridional cir-

culation, as Lindzen and Farrel (1977) have suggested. It is the sensitivity of the states near -1%, and not the relative insensitivity of the larger ice cap states, that requires explanation. The results for $D = 4.0 \times 10^6$ further demonstrate that it is not simply the strength of the diffusivity in midlatitudes that results in the destabilization near -1%, since this value of D is larger than any produced by the dynamic model.

Fig. 10b emphasizes that sensitivity in these constant diffusivity models increases monotonically with decreasing Q, except for slight hitches in the sensitivity curves that have barely visible consequences in Fig. 10a. These small hitches occur when surface albedos of 0.7 first make their appearance as the system is cooled, and can be shown to be remnants of the small ice-cap instability present in discontinuous albedo models. Calculations with various albedo-temperature relations in a one-level model designed to clarify this point are presented in Appendix B. These small hitches are evidently too small to explain the enhanced sensitivity near -1% in the dynamic model.

In Fig. 11 the diffusivity is given latitudinal dependence of the form

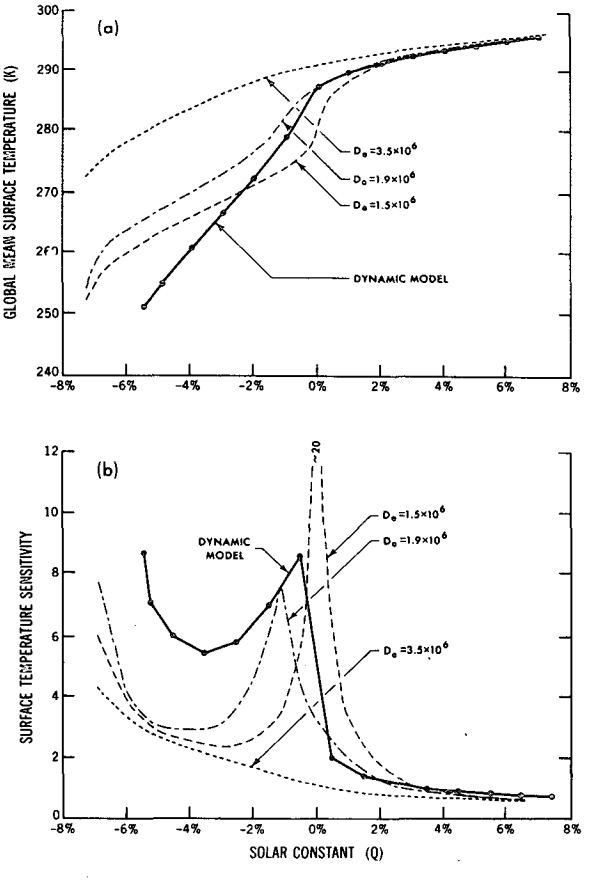

FIG. 11. As in Fig. 10, but for diffusive models with latitudinally varying diffusivities. D_e is the subtropical diffusivity [see Eq. (8)].

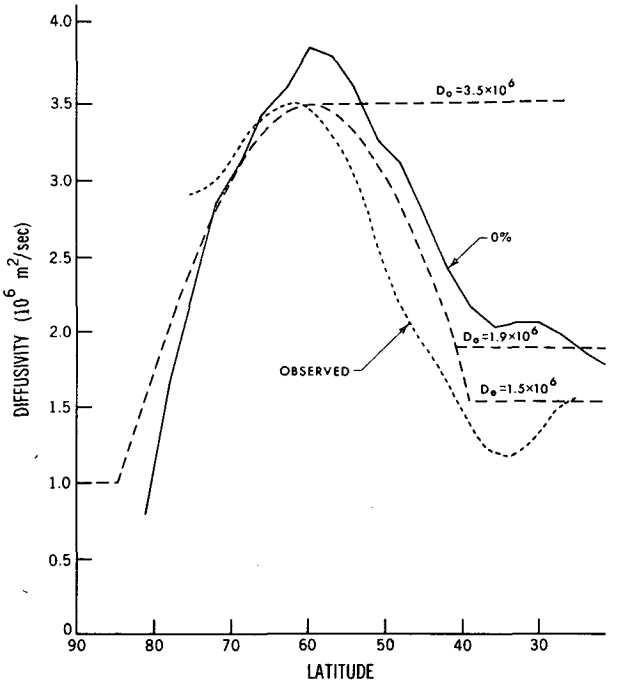

FIG. 12. The latitudinal structure of the effective diffusivity utilized in the calculations described in Fig. 11. The structures resulting from three different choices of D_e are shown (dotted lines). Also shown are the effective diffusivity of the dynamic model at $Q = 0\%$ (solid line) and the diffusivity computed from observed Northern Hemisphere annual mean energy fluxes and 500 mb temperature gradients.

$$D(\theta) = \begin{cases} D_e, & \theta < \theta_e \\ D_m \sin[3(\theta - \pi/6)], & \theta_e < \theta < \theta_p \\ D_p, & \theta_p < \theta \end{cases} \quad (8)$$

where

$$\theta_e = \pi/6 + \tfrac{1}{3} \sin^{-1}(D_e/D_m),$$

$$\theta_p = \pi/2 - \tfrac{1}{3} \sin^{-1}(D_p/D_m).$$

The diffusivity D_p near the pole is set equal to 1.0×10^6 m^2 s^{-1}, and the maximum diffusivity D_m to 3.5×10^6 m^2 s^{-1}. The subtropical diffusivity is given three different values—$D_e = 1.5$, 1.9 and 3.5×10^6 m^2 s^{-1}. This form for the diffusivity is compared with the effective diffusivity of the 0% dynamic calculation in Fig. 12, and also with the observed effective diffusivity of the atmosphere computed from the annual mean atmospheric energy transport and 500 mb temperature gradient in the Northern Hemisphere.[1] (The diffusivities produced by the dynamic model for $Q > 0\%$ are very similar to those for 0%.) The choice of $D_e = 1.9 \times 10^6$ provides a reasonable fit to these dynamic model results. As the figure

[1] Oort, A. H., 1981: Global Atmospheric Circulation Statistics, 1958–1973. NOAA Prof. Pap., U.S. Govt. Printing Office, Washington, D.C. (in preparation).

indicates, this choice of D_e does capture the sensitive region near -1%. We conclude that these sensitive equilibrium states can be interpreted as being a consequence of the structure of the effective diffusivity. A comparison of the $D_e = 1.5 \times 10^6$ and 1.9×10^6 cases in Fig. 11 emphasizes how strongly dependent the sensitivity curves are to this structure.

The diffusive models all underestimate the dynamic model's sensitivity for $Q < -1\%$. This disagreement is not surprising, since the diffusivity changes significantly as the system cools through the -1% transition (as Fig. 9 indicates), and $D(\theta)$ has been chosen to correspond to the warmer cases. However, further calculations show that the agreement between diffusive and dynamic models cannot be improved appreciably by changing the effective diffusivity appropriately as Q changes, unless the errors being made in the vertical distribution of the dynamic heating are simultaneously corrected. Surface cooling due to increased vertical heat flux seems to be primarily responsible for the sensitivity of the large ice-cap states.

The $D_e = 3.5 \times 10^6$ case produces a monotonically increasing sensitivity with decreasing solar constant, emphasizing that the structure of the diffusivity equatorward of 60° is responsible for the enhancement near $Q = -1\%$, and not the structure of the diffusivity near the pole. Also, this version of the model does not produce the small peaks in sensitivity seen in the constant diffusivity models (Fig. 10). These small peaks are sensitive to the structure of the diffusivity near the pole, just as is the small ice-cap instability to which they are related.

The qualitative effect of the diffusivity gradient on sensitivity can be understood by expanding the diffusive heating term

$$\frac{1}{\cos(\theta)} \frac{\partial}{\partial \theta}\left(\cos(\theta) D \frac{\partial \Theta}{\partial \theta}\right) = \frac{D}{\cos(\theta)} \frac{\partial}{\partial \theta}\left(\cos(\theta) \frac{\partial \Theta}{\partial \theta}\right) + \frac{\partial D}{\partial \theta} \frac{\partial \Theta}{\partial \theta} . \quad (9)$$

As Q decreases and the ice cap advances into midlatitudes, the magnitude of the meridional temperature gradient in midlatitudes increases (i.e., $\partial\Theta/\partial\theta$ decreases). As the result, the term proportional to $\partial D/\partial\theta$ in (9) decreases sharply between 60 and 40°, where $\partial D/\partial\theta$ is large and positive. This cooling is compensated in the global mean by the other term in (9); however, if the albedo gradient lies within the region in which the cooling effect is large, then albedo feedback is strengthened. By the same argument, the ice cap should be stabilized when located poleward of 60°, where $\partial D/\partial\theta < 0$; however, the ice cap is then too small for albedo feedback to be of much consequence for the global mean sensitivities in Fig. 11.

b. One-level model

If one is not concerned with closely mimicing the dynamic model, the diffusive model can be simplified drastically and still retain essentially the same behavior. Consider the familiar one-level model with all terms in the energy balance dependent only on "surface temperature":

$$0 = \frac{Q}{4} S(\theta) a(T(\theta)) - (A + BT) + \frac{c'}{a^2 \cos(\theta)} \frac{\partial}{\partial \theta}\left(\cos(\theta) D \frac{\partial T}{\partial \theta}\right) . \quad (10)$$

where $c' = c_p$ (1000 mb/g) $= 1 \times 10^7$ J (m^2 K)$^{-1}$, $s(\theta)$ is the distribution of the annual mean solar flux, normalized so that its global average is unity; $a(T)$ is the planetary co-albedo; and A and B are constants defining the temperature dependence of the outgoing infrared flux. The simplest case is obtained by choosing a discontinuous diffusivity ($D = D_p$ for $\theta > \theta_D$ and $D = D_e < D_p$ for $\theta < \theta_D$) and a discontinuous albedo ($a = \beta$ for $T > T_0$ and $a = \alpha$ for $T < T_0$). The resulting global mean sensitivities are shown in Fig. 13 for the following choice of parameters: $A = 203.3$ W m^{-2} and $B = 2.09$ W (m^2 K)$^{-1}$ (from North and Coakley, 1979); $\theta_D = 45°$; $D_p = 2.5 \times 10^6$ m^2 s^{-1}; $D_e = 2.0 \times 10^6$ m^2 s^{-1}; $\alpha = 0.4$; $\beta = 0.7$; and $T_0 = -10$°C.

The discontinuous albedo produces a small ice-cap instability, reflected in the existence of two possible equilibrium states for $-8.5\% < Q < -7.3\%$. The large ice-cap instability occurs at -11.7%. Results for the ice-covered solutions are not shown. (One can easily increase the values of Q for which stable ice caps exist by decreasing T_0). The sensitivity enhancement for $-10\% < Q < -9\%$ is due to the change in diffusivity and reaches its peak when the ice-cap boundary is located precisely at θ_D. Parameters have been chosen so that this enhancement is clearly distinguished from both the large and small ice-cap instabilities.

The sensitivity enhancement is more prominent when the ice cap is poleward, rather than equatorward, of θ_D. The simple explanation for this behavior is evident from Fig. 14. When the ice cap boundary is poleward of θ_D, the magnitude of the temperature gradient at θ_D increases as the ice cap advances, producing the changes in poleward heat flux shown. These, in turn, result in cooling in the vicinity of θ_D and destabilization of the cap. If the ice cap boundary is further equatorward than θ_D, the magnitude of the temperature gradient at θ_D decreases as the ice cap advances, resulting in warming and stabilization. Equivalently, in response to a perturbation in Q, the contribution of changes in the term $(\partial D/\partial\theta)(\partial T/\partial\theta)$ in (9) to the perturbation global

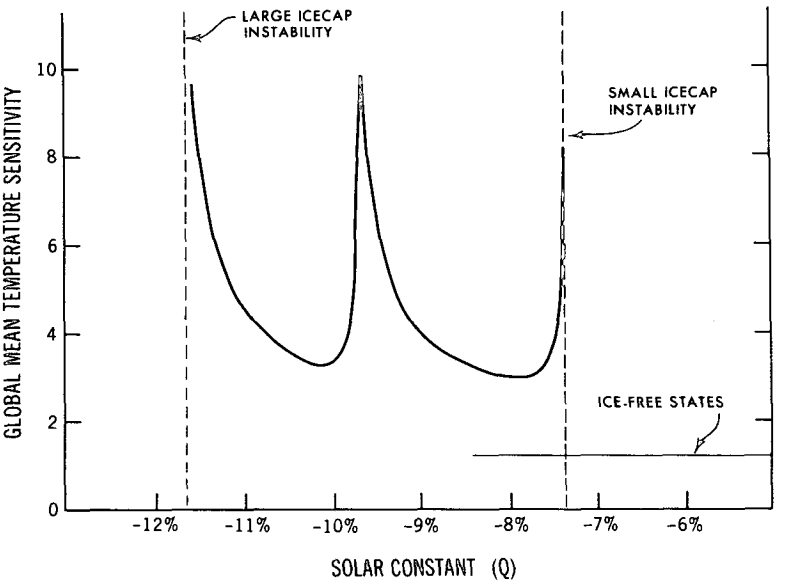

FIG. 13. Sensitivity of global mean temperature to perturbations in Q for the one-level model with discontinuous albedo and discontinuous diffusivity. Sensitivity is defined as in Fig. 10.

energy balance switches sign as the ice cap passes through θ_D.

We hope to have demonstrated with the sequence of energy balance calculations described above that the mechanism pictured in an idealized fashion in Fig. 14 also is responsible for the destabilization in the dynamic model. Of course, the effective diffusivity of the dynamic model does change significantly as Q varies (see Fig. 9), and no claim is being made that the transport is diffusive in any fundamental sense. However, in the absence of a satisfying theory for the poleward heat flux, a latitudinally varying diffusivity does seem to be a convenient way of capturing the characteristic flux responses that result in the peculiar sensitivity curves seen in the dynamic model. There are undoubtedly other ways of capturing this behavior in simple models, a variant of Budyko's model of the sort discussed by Lindzen and Farrell (1977, Section 4) being one possibility.

[It should be noted that the use in a one-level model for surface temperature of a diffusivity approximating that obtained by dividing the atmospheric energy fluxes by the 500 mb temperature gradient is inconsistent. Actually, we feel that all such one-level models should be reinterpreted as models of the mean or mid-tropospheric temperature. In a typical diffusive one-level energy balance model, the diffusivity is sufficiently large that surface temperatures at different latitudes are strongly coupled to each other, and temperature responses to perturbations in Q have only weak latitudinal dependence. However, in both our two-level model and in the Manabe and Wetherald CO_2 (1975, 1980) and solar constant (1975) studies, it is mid-tropospheric temperatures which appear to be strongly coupled and have little

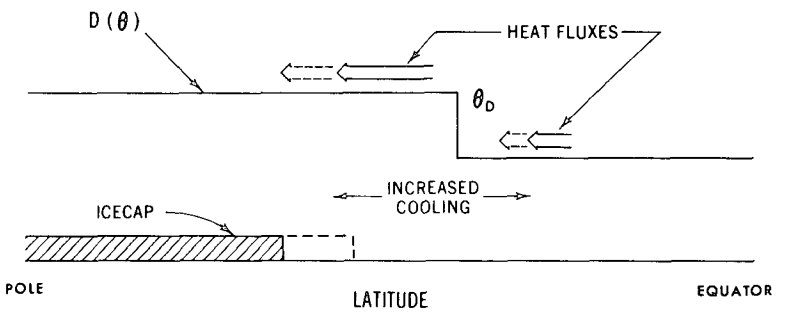

FIG. 14. Schematic of the changes in heat fluxes resulting from an advance of the ice cap, and the resulting cooling in the vicinity of the diffusivity jump.

latitudinal structure in their responses, while surface temperature responses have a great deal of latitudinal structure. The reinterpretation of one-level models as models of mid-tropospheric temperatures requires some modification in the radiative parameterization, but the form $A + BT$ for the outgoing infrared flux, in fact, is a much better approximation if T is taken to be 500 mb rather than surface temperature, as is clear in Fig. 8 of Held and Suarez (1974)].

5. Concluding remarks

The two-level primitive equation atmospheric model described in I and II responds in an intriguing fashion to perturbations in solar constant when albedos are chosen so as to mimic the effects of ice and snow cover. As the system is cooled, but before the large ice cap instability analogous to that found in constant diffusivity energy balance models develops, the system experiences destabilization of another sort. Another still caused by an interplay of albedo feedback and meridional heat transport, the meridional structure of the heat transport (or of the effective diffusivity D) is the key, destabilization occurring when the ice cap boundary enters the region within which $\partial D/\partial\theta$ is positive. Very similar behavior is captured in a two-layer diffusive model closely patterned after the dynamic model. If the latitudinally varying diffusivity in this model is replaced with a latitudinally uniform diffusivity, this destabilization disappears and one is left with a monotonic increase in sensitivity up to the large ice cap instability, except for a weak remnant of the small ice-cap instability. Qualitatively similar behavior also is found in a simple one-level energy balance model.

Whether or not the response of multi-level GCM's is similar to that of this two-level model is an open question. Wetherald (personal communication) indicates that his calculations with Manabe give no sign of producing stable states with the ice cap boundary further equatorward than 40°. Our impression is that if one attempts to mimic these GCM results with a diffusive energy balance model, one will find that the meridional structure of the diffusivity is crucial for the observed destabilization, but that the resulting sensitive states may very well merge continuously into the large ice-cap instability. (Merging of the sensitive states associated with the diffusivity gradient with the large ice-cap instability also explains why calculations in which $D(\theta)$ is chosen proportional to the local temperature gradient (Held and Suarez, 1974; Lin, 1978) do not produce behavior of the sort described here; the diffusivity maxima in these models are located too far equatorward for the diffusivity gradient effects to be significant before the large ice caps become unstable.) Attempts to improve the fit between diffusive and dynamic models described in Fig. 11 suggest that the stability of the large ice-cap states is very sensitive to the details of the response of the horizontal *and vertical* heat fluxes to the passage of the ice cap boundary through the midlatitude maximum in baroclinic activity.

The stability of large ice-cap states is certainly dependent on the response of oceanic as well as atmospheric heat fluxes. If one recomputes the observed effective diffusivity plotted in Fig. 12 using estimates of total oceanic plus atmospheric (rather than only atmospheric) fluxes, one still finds a maximum near 60°N, but the decrease in diffusivity from 60 to 40°N is reduced by a factor of 2. If the oceanic flux behaved at all similarly to diffusion, one could argue on this basis that the oceans would tend to destroy the sensitivity maximum associated with the diffusivity gradient. However, one is tempted to draw the opposite conclusion based on the two-level model's surface wind responses (not shown). The model predicts a modest increase in strength of the surface westerlies equatorward of the ice-cap boundary as the ice cap expands. One therefore expects a stronger equatorward Ekman drift of warm surface waters in this region, resulting in cooling at the boundary of the advancing ice cap and an associated increase in sensitivity if this is the dominant effect. Thus, the possibility exists for either significant stabilization or destabilization by the oceanic flux response.

It is tempting to speculate on the paleoclimatic significance of the existence of sensitive states not associated with the large ice-cap instability. Any effect which significantly increases climatic sensitivity as the system is cooled without requiring one to be perched on the brink of the large ice-cap instability is certainly of potential significance for ice age theories, but plausible arguments relating the ice ages to these sensitive states must await calculations with more convincing climate models.

Acknowledgments. The authors would like to thank S. Manabe, R. Wetherald, K. Bryan and A. Oort for their comments and assistance, the Scientific Illustration Group at GFDL for the figures, and Joyce Kennedy for typing the manuscript. One of the authors (MJS) was supported by the National Science Foundation under Grant ATM77-28114.

APPENDIX A

The Radiative Flux Computation

The calculations on which the following algorithms are based are described in I. The upward flux L_1 of infrared radiation at the top of the atmosphere, the net upward flux L_2 at 500 mb and the downward flux L_3 at the surface are computed from

$$L_i = a_i(\bar{\Theta}) + b_i(\bar{\Theta})\hat{\Theta} + c_i(\bar{\Theta})\Delta T, \quad i = 1, 3. \quad \text{(A1)}$$

TABLE A1. Values of the parameters required for the infrared flux computation. The units of a_i, b_i and c_i are W m^{-2}, W (m^2 K)$^{-1}$ and W (m^2 K)$^{-1}$, respectively.

$\bar{\Theta}$ (°C)	a_1	b_1	c_1	a_2	b_2	c_2	a_3	b_3
−30	109.0	−1.10	1.00	121.3	−2.18	1.26	104.3	−1.72
−25	118.0	−1.16	1.01	131.0	−2.29	1.25	119.1	−2.06
−20	127.4	−1.22	1.01	140.8	−2.38	1.25	134.7	−2.37
−15	136.9	−1.26	1.01	150.6	−2.47	1.25	150.9	−2.65
−10	146.8	−1.30	1.01	160.0	−2.52	1.26	167.8	−2.91
−5	156.8	−1.34	1.01	168.3	−2.55	1.26	185.7	−3.17
0	167.2	−1.37	1.01	176.4	−2.60	1.26	204.9	−3.44
5	177.6	−1.40	1.01	183.7	−2.64	1.25	225.7	−3.74
10	188.3	−1.42	0.99	190.6	−2.68	1.24	248.1	−4.06
15	199.2	−1.43	0.97	197.0	−2.72	1.21	271.9	−4.40
20	210.0	−1.44	0.95	202.8	−2.74	1.18	297.1	−4.74
25	221.0	−1.44	0.92	208.1	−2.75	1.15	323.6	−5.08
30	232.1	−1.43	0.88	213.1	−2.76	1.10	351.8	−5.45
35	243.2	−1.41	0.83	217.6	−2.75	1.04	382.4	−5.85
40	254.2	−1.39	0.77	221.7	−2.73	0.96	415.7	−6.32
45	265.0	−1.35	0.68	225.0	−2.69	0.85	452.0	−6.85
50	275.6	−1.30	0.59	227.8	−2.65	0.74	491.4	−7.43
55	286.1	−1.24	0.48	230.2	−2.60	0.61	533.7	−8.04
60	296.2	−1.16	0.39	231.9	−2.53	0.48	578.3	−8.66
65	306.0	−1.08	0.30	233.0	−2.45	0.37	624.7	−9.25
70	315.6	−0.98	0.24	233.6	−2.36	0.29	672.2	−9.79

The functions a_i, b_i, c_i, dependent only on $\bar{\Theta} \equiv \frac{1}{2}(\Theta_1 + \Theta_2)$, are obtained by linearly interpolating on Table A1 (except for c_3, which is identically zero). In (A1), $\hat{\Theta} \equiv \frac{1}{2}(\Theta_1 - \Theta_2)$ and $\Delta T \equiv T_* - T_A$, the latter being the temperature jump at the ground. (There are several errors in the corresponding table in I. The values actually used for the computations described in I are those listed here in Table A1). The longwave heating of the upper and lower layers is then given by

$$\left.\begin{aligned} Q_1^{LW} &= (L_2 - L_1)/C \\ Q_2^{LW} &= (\sigma T_*^4 - L_3 - L_2)/C \end{aligned}\right\}, \qquad \text{(A2)}$$

where C is defined as in (7).

If S is the incident solar flux at the top of the atmosphere, the flux Ss_0 is reflected to space by molecular scattering; Ss_1 is reflected to space by clouds in the upper layer; Ss_2 is transmitted through the upper layers, reaching 500 mb; Ss_3 is reflected from clouds in the lower layer; and Ss_4 reaches the ground. If γ is the surface albedo, γSs_4 is reflected by the surface, while γSs_5 is that part of this reflected flux escaping to space, the remainder being absorbed in the lower layer (the absorption of reflected radiation in the upper layer being neglected). These relations are depicted in Fig. A1. The s_i are determined from expressions linear in $\bar{\Theta}$ and $\hat{\Theta}$:

$$s_i = d_i + (\bar{\Theta} - 300\ \text{K})e_i + \hat{\Theta} f_i, \quad i = 2\text{–}5, \qquad \text{(A3)}$$

where d_i, e_i and f_i are functions only of Z, the cosine of the zenith angle, as listed in Table A2. $s_0 + s_1$ is simply set equal to 0.10. The incident flux is given

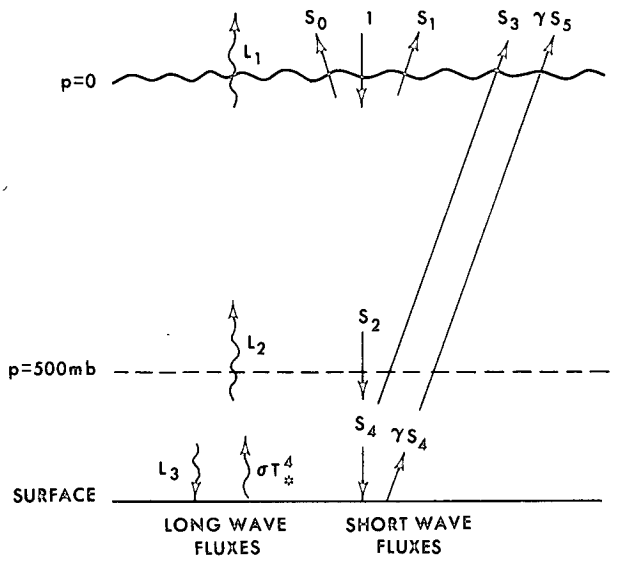

FIG. A1. Schematic of the radiative flux computation.

its annual mean values as a function of latitude, $0.25Qs(\theta)$. A plot of $s(\theta)$ for the obliquity used (23.5°) can be found in Held and Suarez (1974). The effective annual mean cosine of the zenith angle is approximated by averaging its instantaneous value, weighted by the instantaneous insolation, over the diurnal and annual cycles; it ranges from 0.3 at the pole to 0.6 at the equator. The solar heating of the upper and lower layers is given by

TABLE A2. Values of the parameters required for the solar heating computation. Z is the cosine of the zenith angle. The units of e_i and f_i are 10^{-3} K^{-1}; d_i is dimensionless.

Z		$i = 2$	$i = 3$	$i = 4$	$i = 5$
0.1	d_i	0.821	0.182	0.481	0.477
	e_i	−1.13	−0.45	−1.62	−1.62
	f_i	0.08	0.18	1.41	1.44
0.2	d_i	0.835	0.186	0.497	0.490
	e_i	−0.96	−0.42	−1.56	−1.59
	f_i	0.07	0.16	1.28	1.34
0.3	d_i	0.842	0.188	0.506	0.497
	e_i	−0.86	−0.40	−1.52	−1.56
	f_i	0.06	0.15	1.20	1.28
0.4	d_i	0.847	0.189	0.513	0.502
	e_i	−0.80	−0.39	−1.49	−1.54
	f_i	0.05	0.15	1.04	1.24
0.5	d_i	0.851	0.190	0.518	0.505
	e_i	−0.76	−0.38	−1.46	−1.53
	f_i	0.05	0.14	1.09	1.22
0.6	d_i	0.853	0.191	0.522	0.506
	e_i	−0.72	−0.37	−1.43	−1.52
	f_i	0.05	0.14	1.05	1.20
0.7	d_i	0.856	0.192	0.525	0.509
	e_i	−0.69	−0.37	−1.41	−1.51
	f_i	0.05	0.14	1.02	1.18

$$\left.\begin{aligned} Q_1^{SW} &= \tfrac{1}{4}Qs(\theta)(1 - s_0 - s_1 - s_2)/C \\ Q_2^{SW} &= \tfrac{1}{4}Qs(\theta)(s_2 - s_3 - s_4(1-\gamma) - \gamma s_5)/C \end{aligned}\right\}, \quad \text{(A4)}$$

while the net radiative flux at the ground needed in the surface energy balance is

$$s_\downarrow = L_3 - \sigma T_*^4 + \tfrac{1}{4}Qs(\theta)s_4(1-\gamma), \quad \text{(A5)}$$

$$a(T) = \begin{cases} 0.7, & T > T_0 + 0.5\Delta T \\ 0.55 + 0.30(T - T_0)/\Delta T, & T_0 + 0.5\Delta T > T > T_0 - 0.5\Delta T \\ 0.4, & T_0 - 0.5\Delta T > T \end{cases} \quad \text{(B1)}$$

As $\Delta T \to 0$, this reduces to the model possessing a small ice cap instability considered in Held and Suarez (1974) and North (1975). The sensitivities for $\Delta T = 2.5$, 5.0 and 10.0 K, are plotted in Fig. B1.

A rather small amount of smoothing is sufficient to eliminate the small ice-cap instability and the associated non-uniqueness of equilibrium states. The case $\Delta T = 2.5$ is very close to the point at which the instability disappears, as is evident in the very small range of Q for which two equilibrium states exist. The instability has been eliminated in the $\Delta T = 5.0$ case, but there remains a peak in sensitivity near the value of Q at which instability occurs for smaller ΔT. For the still larger value $\Delta T = 10.0$, there remains only a trace of the global mean sensitivity enhancement associated with this instability.

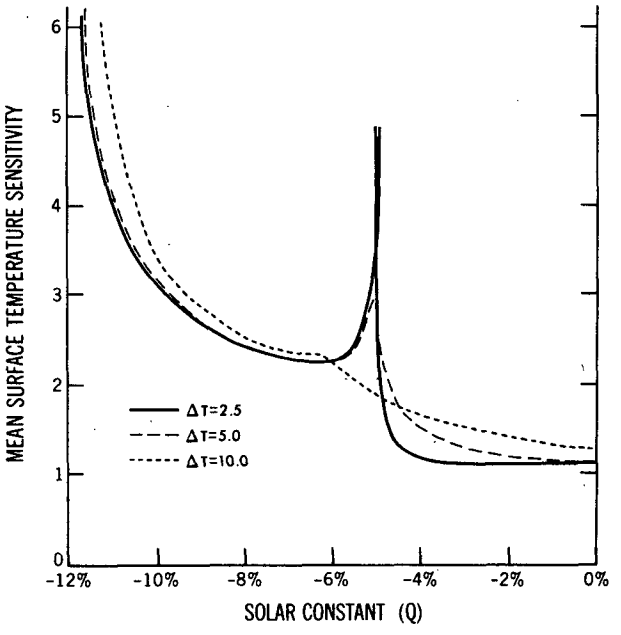

FIG. B1. Sensitivity of global mean temperature to changes in Q, as a function of Q, for one-level uniform diffusivity models with different amounts of albedo smoothing. ΔT is defined in (B1). Sensitivity is defined as in Fig. 10.

APPENDIX B

Albedo Smoothing and the Small Ice-Cap Instability

Consider the simplest one-level energy balance model (10) with a uniform diffusivity $D = 2.0 \times 10^6$ m^2 s^{-1}, with the same radiative parameters A and B as in Section 4b, but with an albedo-temperature relation of the form

The case $\Delta T = 5.0$ most closely resembles the results in Fig. 10 for the two-layer uniform diffusivity models with $\Delta T = 10.0$ K. Variable static stability evidently enhances the small ice-cap instability, the increase in static stability with decreasing solar constant increasing the sensitivity of high latitude surface temperatures.

We have not displayed the results obtained by decreasing ΔT in the two-layer diffusive model because these calculations introduce yet another confusing aspect of albedo-feedback models that is not directly related to the questions addressed in this paper. The two-layer model actually possesses a continuum of possible equilibrium states at a given Q if ΔT is sufficiently small. This peculiar property is a simple consequence of the fact that the model can support a discontinuity in surface temperature at a surface albedo discontinuity, although atmospheric temperatures are necessarily continuous. The size of the surface discontinuity is dependent on the strength of the coupling between surface and atmospheric temperatures. The proof that such a discontinuity results in a continuum of equilibrium states is identical to that given for Budyko's model in Held and Suarez (1974). While we believe that this direct consequence of the sharp surface temperature gradients associated with sharp albedo gradients is of some physical interest, we have chosen to omit a discussion of this point here.

REFERENCES

Budyko, M. I., 1969: The effect of solar radiation variations on the climate of the earth. *Tellus*, **21**, 611–619.

Hartmann, D. L., and D. A. Short, 1979: On the role of zonal asymmetries in climate change. *J. Atmos. Sci.*, **36**, 519–528.

Held, I. M., 1978: The tropospheric lapse rate and climatic sensitivity experiments with a two-level atmospheric model. *J. Atmos. Sci.*, **35**, 2083–2098.

——, and M. J. Suarez, 1974: Simple albedo feedback models of the ice caps. *Tellus*, **26**, 613–629.

——, and ——, 1978: A two-level primitive equation atmospheric model designed for climatic sensitivity experiments. *J. Atmos. Sci.*, **35**, 206–229.

Lin, C. A., 1978: The effect of nonlinear diffusive heat transport in a simple climate model. *J. Atmos. Sci.*, **35**, 337–340.

Lindzen, R. S., and B. Farrell, 1977: Some realistic modifications of simple climate models. *J. Atmos. Sci.*, **34**, 1487–1501.

Manabe, S., and R. T. Wetherald, 1975: The effects of doubling the CO_2 concentration on the climate of a general circulation model. *J. Atmos. Sci.*, **32**, 3–15.

——, and ——, 1980: On the horizontal distribution of climate change resulting from an increase in CO_2 content of the atmosphere. *J. Atmos. Sci.*, **37**, 99–118.

North, G. R., 1975: Analytical solution to a simple climate model with diffusive heat transport. *J. Atmos. Sci.*, **32**, 1301–1307.

——, and J. A. Coakley, 1979: Differences between seasonal and mean annual energy balance model calculations of climate and climate sensitivity. *J. Atmos. Sci.*, **36**, 1189–1204.

Oerlemans, J., and H. M. van den Dool, 1978: Energy balance climate models: stability experiments with a refined albedo and updated coefficients for infrared emission. *J. Atmos. Sci.*, **35**, 371–381.

Oort, A. H., and E. M. Rasmussen, 1971: Atmospheric circulation statistics. NOAA Prof. Pap. No. 5, [U.S. Govt. Printing Office, Stock No. 0317-0045, C55.25:S], 323 pp.

Sellers, W. D., 1969: A global climatic model based on the energy balance of the earth-atmosphere system. *J. Appl. Meteor.*, **8**, 392–400.

Suarez, M. J., and I. M. Held, 1979: The sensitivity of an energy balance climate model to variations in the orbital parameters. *J. Geophys. Res.*, **84**, 4825–4836.

Wang, W. C., and P. H. Stone, 1980: Effect of ice-albedo feedback on global sensitivity in a one-dimensional radiative-convective climate model. *J. Atmos. Sci.*, **37**, 545–552.

Wetherald, R. T., and S. Manabe, 1975: The effects of changing the solar constant on the climate of a general circulation model. *J. Atmos. Sci.*, **32**, 2044–2059.